Development of Ar I and Ar II Measuring System using Laser-Induced Fluorescence Methods in High-Density Helicon Plasma[*]

Daisuke KUWAHARA, Yuriko TANIDA, Masaki WATANABE[1], Naoto TESHIGAHARA, Yukihiko YAMAGATA[2] and Shunjiro SHINOHARA

Tokyo University of Agriculture and Technology, 2-24-16 Naka-Cho, Koganei, Tokyo 184-8588, Japan
[1]*Tokyo Institute of Technology, 2-12-1 Ookayama, Meguro, Tokyo 152-8550, Japan*
[2]*Kyushu University, 6-1 Kasuga-Koen, Kasuga, Fukuoka 816-8580, Japan*

A particle flow velocity measurement is important to realize a behavior of exhausted plasma in an electric thruster. Laser-induced fluorescence (LIF) method provides flow velocities of ions and neutral particles through measuring velocity distribution functions of them. In addition, LIF method has some advantages, shown as follows; 1) high-spatial resolution, 2) absolute measurement of flow velocity, 3) direction-selectivity of velocity distribution functions. We have developed Ar I and Ar II LIF measuring system to observe spatial profiles of velocity distribution functions of both neutral particles and ions in an experimental device of the helicon plasma thruster, having permanent magnets as the applied magnetic field. Flow velocity of the neutral particle in the axial direction was subsonic, and ion velocity was related with a gradient of the magnetic field.

1. Introduction

In most practical use of electric thrusters such as a Hall thruster, an ion engine and a MPD thruster, there is a problem of a life-time limitation due to erosions of electrodes which contact with plasma directly. To solve this problem, our group has proposed a completely electrodeless electric thruster using a high-density helicon plasma [1]. The helicon plasma thruster has a potential to be a long-lifetime and a high-thrust propulsion system, such as a main thruster for a deep space explorer. Schemes of the helicon plasma thruster are as follows: 1) to generate high-density plasma using an antenna installed outside of a discharge tube so-called "electrodeless" conditions, 2) to accelerate the plasma with also electrodeless conditions, 3) to exhaust the plasma into space. In generating the plasma, helicon plasma [1, 2] has many advantages. This plasma is one of the radio-frequency (RF) plasmas under the magnetic field, and its particle production efficiency N_e/P_{inp} (N_e; total number of electrons produced, P_{inp}: input RF power) [3] is sufficiently high. In the phase of acceleration, the plasma must be exhausted with a high-speed to the direction of the exit. There are acceleration forces, e.g., a density gradient ∇n, and a magnetic gradient $-\mu\nabla B$ (both gradients have the axial direction), where n, μ and B indicate an electron density, a magnetic moment and the applied magnetic field. The density gradient is naturally exists when the plasma is generated, and the magnetic gradient also exists in the open-end of the parallel magnetic field (magnetic nozzle). In addition, our group has been studying some active acceleration methods to improve the thrust efficiency. These methods produce an axial direction thrust F_z using the Lorentz force, i.e., the product of an induced azimuthal current j_θ and an external radial magnetic field B_r [1, 4, 5].

In studying the above-mentioned schemes, it is important to observe behaviors of particles such as ions and neutral particles, playing the role of the thrust production. Here, we have been developing a laser-induced fluorescence (LIF) method to observe flow velocities and temperatures of ions and neutral particles. If flow velocities of whole particles in plasma are observed, the total thrust can be estimated. In our previous research, a LIF measurement system was developed to observe the axial flow velocity and temperature of argon ion [6]. However, the total thrust consists of contributions of ion and neutral particles. Therefore, to obtain the whole particle behaviors to estimate the total force and to optimize the thrust performance, it is essential to develop a LIF system observing neutral particles as well.

2. Principle of LIF Measurement

Figure 1 shows LIF schemes of the ion and the neutral

particle. For an argon ion, we use a three state scheme, in which Ar II 3d^{4}F$_{7/2}$ metastable state is optically pumped by 668.63 nm (in vacuum) laser light to 4p^{4}D$_{5/2}$ state, which decays to 4 s^{4}P$_{3/2}$ state by an emission at 442.73 nm [7]. For an argon neutral particle, Ar I 4s(^{2}P$^0_{3/2}$)$_1$ metastable state is optically pumped by 667.92 nm (in vacuum) laser light to 4p$'$(^{2}P$^0_{1/2}$)$_0$ state, which decays to 4s$'$(^{2}P$^0_{1/2}$)$_1$ state by an emission at 750.61 nm [8]. Note that using targets of the neutral particle and ion schemes are metastable states, and these schemes cannot measure the ground state of the neutral particle and ion. If target particles move in a direction of the pumping laser axis, its absorption wavelengths are changed by the Doppler shift. The LIF measurement system can obtain particle velocity distribution function by detecting LIF intensities at each resonant wavelength. Flow velocity and temperature of the target particles are obtained from the Doppler shift and the full width at half maximum of the velocity distribution function, respectively, as shown in Eqs. (1) and (2):

$$v = c\Delta\nu/\nu_0, \tag{1}$$

$$T = \frac{1}{8\ln 2}\frac{mc^2}{k_B}\frac{\nu_{FWHM}^2}{\nu_0{}^2}. \tag{2}$$

Here, v is the particle flow velocity, c the speed of light, $\Delta\nu$ the frequency shift due to the Doppler effect, ν_0 the resonant frequency of the particle at rest, T the temperature of the particle, $\Delta\nu_{FWHM}$ the full width at half maxi-
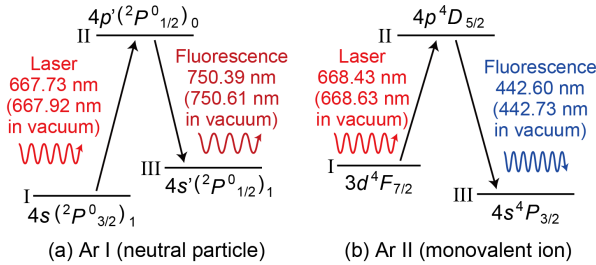
mum of its Doppler spectrum, m the particle mass, and k_B the Boltzmann constant.

3. Experimental Setup

Figure 2 shows a schematic diagram of Large Mirror Device (LMD) [9]. A quartz discharge tube [1,000 mm in length and 100 ~ 170 mm in inner diameter (i.d.)] has a tapered shape to prevent a wall loss of plasmas, and the tube is connected to a vacuum chamber (1,700 mm in length and 445 mm in i.d.). LMD has two turbo-molecular pumps (1,000 l/s and 2,400 l/s) with a base pressure < 10^{-4} Pa. Argon gas was used as a propellant one, and a typical discharge pressure was > 1 Pa. Plasma is generated by a RF power via a half-helical antenna. The RF input power P_{RF} and its excitation frequency f_{RF} were ~ 3 kW and 7 MHz, respectively. There are two types of applied magnetic field system, permanent magnets and electromagnets. In this paper, only permanent magnets were used [5]. Permanent magnets which were placed in the discharge tube straight section generate a large magnetic field in a radial direction.

For an excitation laser, a tunable laser diode system (TA100, TOPTICA Photonics AG) has been utilized. The system has an oscillator and an amplifier internally, and the tuning range of the laser wavelength and bandwidth are 663.5 ~ 669.3 nm and ~ 1 MHz, respectively. Scanning bandwidth for Ar I and Ar II measurements were 448,848 ~ 448,851 THz and 448,368 ~ 448,382 THz, respectively. The typical output power of the laser was ~ 200 mW in this experiment. Wavelength of the laser was measured with a wavelength meter (WS7, High Finesse GmbH, absolute accuracy: 60 MHz). Absolute calibrations of wavelength, i.e. fundamental wavelengths of both Ar I and Ar II were decided by the middle point between Doppler shifts by the forward and backward laser injection using a reflecting mirror [10]. In addition, our system can exclude a power-broadening problem of Doppler spectrum, because of the low power density of the pumping laser. In order to detect the small LIF signal above the large noise, the laser light is electrically modulated at

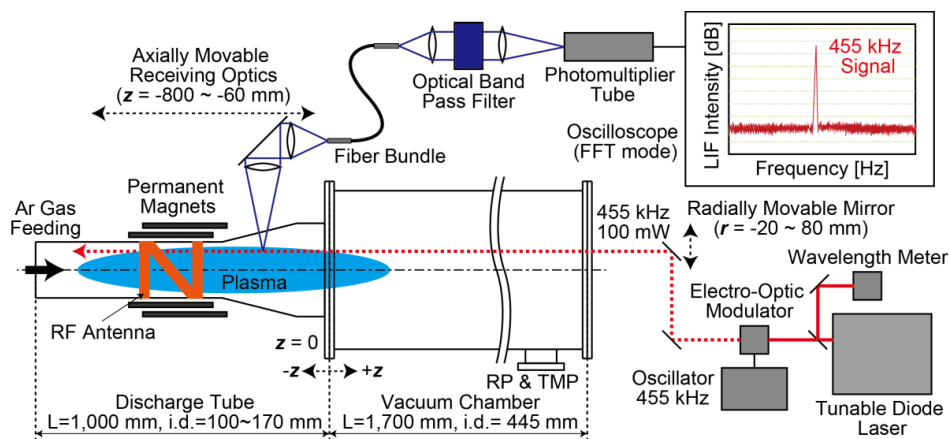Fig. 1   Three-state LIF schemes of Ar I (argon neutral particle) and Ar II (argon monovalent ion).

Fig. 2   Schematic of LMD and LIF system.

455 kHz frequency by the use of Electro-Optic Modulators (LM0202, Qioptiq). This frequency was the same as a frequency of a local oscillation of the AM Radio; therefore a narrow-band band-pass filter can be obtained inexpensively. The diameter of the injected laser was ~ 2 mm, and the axial length of the measurement range of receiving optics was ~ 5 mm. Thus, the observed volume was ~ 16 mm^3. The fluorescent emission is collected by a receiving optics and a fiber bundle cable. The receiving optics and the injected laser one can be moved in synchronization with 2D measurements in the axial and the radial directions. The observation area of the receiving optics was −70 ~ −650 mm in the axial direction and −20 ~ 80 mm in the radial one. In this experiment, the direction of the velocity distribution function was only the axial component. The collected LIF passes through 1 nm and 4 nm bandwidth interference filters for Ar I and Ar II measurements, respectively. Here, the center wavelengths for the Ar I and the Ar II measurements were 750.6 nm and 442.6 nm, respectively. Two types of high-gain photomultiplier tubes (PMT) are used as LIF detectors. Because of their sensitivity characteristics, photomultipliers of R943-02 and H7422-40 (Hamamatsu Photonics) were used for Ar I and Ar II, respectively. In order to separate LIF signal from background radiations, natural emission and electric noise, we employed a narrow-band band-pass filter (CFWLB455KFFA-B0, Murata Manufacturing Co., Ltd.) and a Fast Fourier Transform (FFT) method. The LIF signal was observed using a high-speed oscilloscope (WaveSurfer 104MXs-A, Teledyne LeCroy Japan Corporation).
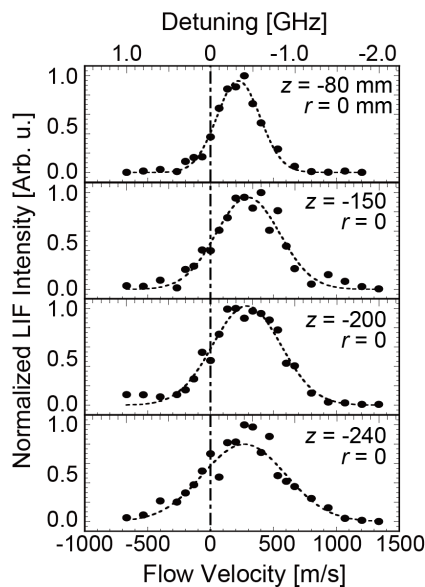
4. Experimental Results

Figure 3 shows an example of neutral particle (Ar I) measurements. Here, because the axis of the pumping lasers was oriented parallel to the magnetic field, and the polarization of the laser was the linear one, $\pm\sigma$ transitions were occurred. However, in our experimental condition, Zeeman shifts for neutral particles and ions are ± 1.4 GHz/kG and ± 0.6 GHz/kG, respectively [8, 11]. Since these shifts are smaller than Doppler broadenings, each flow velocity can be evaluated from the single Gaussian fitting curve. The vertical axis indicates LIF intensities (normalized), the horizontal axis the flow velocity and the detuning of laser frequency, and the dotted lines Gaussian fitting curves. Discharge parameters are as follows; $P_{RF} = 500$ W, gas flow rate $FR = 90$ sccm (Ar pressure $P_{Ar} = 0.8$ Pa), measurement points $z = -80 \sim -240$ mm (center of $r = 0$ mm was fixed). In this experiment, axial velocities of neutral particle indicated subsonic in the downstream of the RF antenna. The flow velocities did not change appreciably regardless of the axial position. The temperature of neutral particles was roughly equal to the room temperature, and it was lower in a downstream region.

Figure 4 shows an example of ion (Ar II) measurements. Discharge parameters are as follows; $P_{RF} = 2,000$ W, $FR = 50$ sccm ($P_{Ar} = 0.6$ Pa), measurement points $r = 0 \sim 60$ mm (axial position of $z = -240$ mm fixed). Flow velocities of argon ion were considerably higher than those of neutral particle, and the temperature of ions was about ~ 0.5 eV. Here, in the edge region ($r = 40$ and 60 mm), intensities of LIF were smaller than that in the center region (data not shown), suggesting the lower ion density in the edge region.

Figure 5 shows flow velocities of neutral particles. Discharge parameters are as follows; $P_{RF} = 500$ and

Fig. 3   Neutral particle (Ar I) velocity distribution functions in the axial direction. [P_{RF}: 500 W, FR: 90 sccm (pressure: 0.8 Pa)].
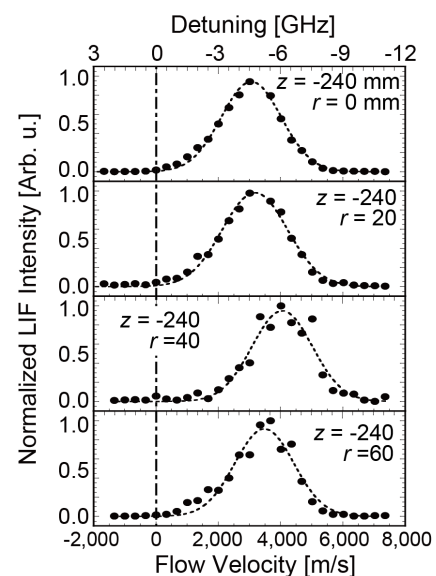

Fig. 4   Ion (Ar II) velocity distribution functions in the axial direction. [P_{RF}: 2,000 W, FR: 50 sccm (pressure: 0.6 Pa)].

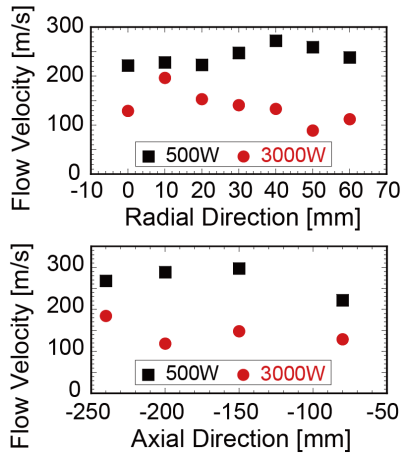Fig. 5 Flow velocities of neutral particles in radial ($z = 80\,\mathrm{mm}$) and axial ($r = 0\,\mathrm{mm}$) directions (P_{RF}: 500 & 3,000 W, FR: 90 sccm (0.8 Pa).
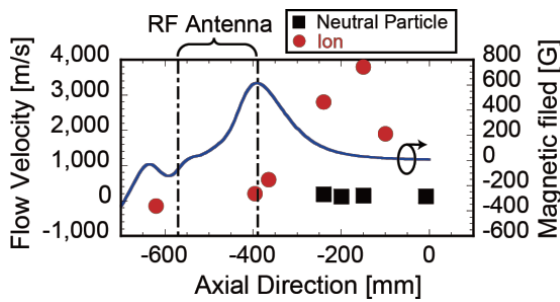

Fig. 6 Flow velocities of neutral particles and ions in axial directions ($r = 0\,\mathrm{mm}$), and magnetic field strength distributions. (P_{RF}: 3,000 W, and FR: 50 sccm (0.6 Pa)).

3,000 W, $FR = 90\,\mathrm{sccm}$ ($P_{\mathrm{Ar}} = 0.8\,\mathrm{Pa}$), measurement points $r = 0 \sim 60\,\mathrm{mm}$, $z = -80 \sim -240\,\mathrm{mm}$). Flow velocities did not change appreciably again (especially $P_{\mathrm{rf}} = 500\,\mathrm{W}$ case), regardless of the axial and radial positions in each P_{RF} case. However, flow velocity of $P_{\mathrm{rf}} = 3,000\,\mathrm{W}$ ones were smaller than 500 W cases.

Figure 6 shows axial flow velocity distributions of neutral particles and ions. Discharge parameters are as follows; $P_{\mathrm{RF}} = 3,000\,\mathrm{W}$, $FR = 50\,\mathrm{sccm}$ ($P_{\mathrm{Ar}} = 0.6\,\mathrm{Pa}$), measurement points $z = -80 \sim -240\,\mathrm{mm}$ (neutral particle), $z = -620 \sim -100\,\mathrm{mm}$ (ion), and $r = 0\,\mathrm{mm}$ (fixed). The left vertical axis and the right one indicate the flow velocities of ions and neutrals, and the magnetic field strength, respectively. Ion velocities were sufficiently accelerated around $z = -400 \sim -140\,\mathrm{mm}$, where the negative magnetic gradient exists. The increasing of the ion velocity is considered to be due to $-\mu\nabla B$ acceleration. On the other hand, the velocity of neutral particles was not changed despite of the ion velocity being changed. It is important to estimate the relation between neutral particles and ions from the viewpoint of the momentum transfer through collisions for future studies.

Here, we try to calculate the plasma thrust and specific impulse by the use of flow velocities of neutral particle and the ions by the LIF method, the neutral particle density calculated by FR, and the ion density observed by a Langmuir probe. Using Eqs. (3) and (4), each thrust can be calculated.

$$F_{\mathrm{n}} = \dot{m}_{\mathrm{n}} v_{\mathrm{n}}, \tag{3}$$

$$F_{\mathrm{i}} = n_{\mathrm{i}} m_{\mathrm{i}} v_{\mathrm{i}}^2 \pi a^2. \tag{4}$$

Here, F_{n}, F_{i}, $\dot{m}_{\mathrm{n}}$, v_{n}, v_{i}, n_{i}, m_{i}, a indicates thrusts coming from neutral particles and ions, mass flow rate of neutral particles, flow velocities of neutral particles and ions, the ion density, mass of the ion, and the radius of a discharge tube. Input values are as follows; $P_{\mathrm{RF}} = 3,000\,\mathrm{W}$, $\dot{m}_{\mathrm{n}} = 30\,\mathrm{sccm}$ ($9.0 \times 10^{-7}\,\mathrm{kg/s}$), $v_{\mathrm{n}} = 240\,\mathrm{m/s}$, $v_{\mathrm{i}} = 3,000\,\mathrm{m/s}$, $n_{\mathrm{i}} = 1 \times 10^{18}\,\mathrm{m}^{-3}$, $m_{\mathrm{n}} = 6.7 \times 10^{-26}\,\mathrm{kg}$, $a = 0.05\,\mathrm{m}$. This leads to F_{n} and F_{i}, of ~ 0.2 and $\sim 4.7\,\mathrm{mN}$, respectively. The total thrust of $\sim 4.9\,\mathrm{mN}$ ($P_{\mathrm{RF}} = 3,000\,\mathrm{W}$, $\dot{m}_{\mathrm{n}} = 30\,\mathrm{sccm}$) is consistent with the thrust observed by a target-type thrust installed in $z = 20\,\mathrm{mm}$.

5. Conclusion

In order to estimate the advanced electromagnetic acceleration method, we have been developing the LIF system which can observe both the neutral particle and ion velocity distribution functions. The LIF system can also observe spatial profiles of these functions in the axial and radial directions in the discharge tube region. Preliminary measurement results showed that neutral flow velocities of $P_{\mathrm{RF}} = 500\,\mathrm{W}$ cases were subsonic, and those were decreased for cases of $P_{\mathrm{RF}} = 3,000\,\mathrm{W}$. Here, ions were accelerated in the negative magnetic gradient region. The total thrust calculated by LIF measurements was consistent with the thrust stand measurement.

Acknowledgments

[1] S. Shinohara *et al.*, IEEE Trans. Plasma Sci. **42**, 1245 (2014).
[2] R.W. Boswell, Phys. Lett. **33A**, 457 (1970).
[3] S. Shinohara *et al.*, Phys. Plasmas **16**, 057104 (2009).
[4] T. Ishii *et al.*, JPS Conf. Proc. **1**, 015047 (2014).
[5] S. Otsuka *et al.*, Plasma Fusion Res. **9**, 3406047 (2014).
[6] N. Teshigahara *et al.*, Plasma Fusion Res. **9**, 3406055 (2014).
[7] R.F. Boivin *et al.*, Rev. Sci. Instrum. **74**, 4352 (2003).
[8] A.M. Keesee *et al.*, Rev. Sci. Instrum. **75**, 4097 (2004).
[9] S. Shinohara *et al.*, Jpn. J. Appl. Phys. **35**, 4503 (1996).
[10] S. Yoshimura *et al.*, Plasma Fusion Res. **5**, S2052 (2010).
[11] A.M. Keesee *et al.*, Phys. Plasmas **12**, 093502 (2005).
[12] D. Kuwahara *et al.*, Plasma Fusion Res. **9**, 3406025 (2014).